Protoplasma (2012) 249:687–697
DOI 10.1007/s00709-011-0312-3

ORIGINAL ARTICLE

Callose deposition in the phloem plasmodesmata and inhibition of phloem transport in citrus leaves infected with "*Candidatus Liberibacter asiaticus*"

Eun-Ji Koh · Lijuan Zhou · Donna S. Williams · Jiyoung Park · Ningyuan Ding · Yong-Ping Duan · Byung-Ho Kang

Received: 5 May 2011 / Accepted: 17 June 2011 / Published online: 28 August 2011

Abstract Huanglongbing (HLB) is a destructive disease of citrus trees caused by phloem-limited bacteria, *Candidatus Liberibacter* spp. One of the early microscopic manifestations of HLB is excessive starch accumulation in leaf chloroplasts. We hypothesize that the causative bacteria in the phloem may intervene photoassimilate export, causing the starch to over-accumulate. We examined citrus leaf phloem cells by microscopy methods to characterize plant responses to *Liberibacter* infection and the contribution of these responses to the pathogenicity of HLB. Plasmodesmata pore units (PPUs) connecting companion cells and sieve elements were stained with a callose-specific dye in the *Liberibacter*-infected leaf phloem cells; callose accumulated around PPUs before starch began to accumulate in the chloroplasts. When examined by transmission electron microscopy, PPUs with abnormally large callose deposits were more abundant in the *Liberibacter*-infected samples than in the uninfected samples. We demonstrated an impairment of symplastic dye movement into the vascular tissue and delayed photoassimilate export in the *Liberibacter*-infected leaves. *Liberibacter* infection was also linked to callose deposition in the sieve plates, which effectively reduced the sizes of sieve pores. Our results indicate that *Liberibacter* infection is accompanied by callose deposition in PPUs and sieve pores of the sieve tubes and suggest that the phloem plugging by callose inhibits phloem transport, contributing to the development of HLB symptoms.

Keywords *Candidatus Liberibacter asiaticus* · Huanglongbing · Plasmodesmata · Plasmodesmata pore unit · Callose · Phloem

Handling Editor: Manfred Heinlein

Electronic supplementary material The online version of this article (doi:10.1007/s00709-011-0312-3) contains supplementary material, which is available to authorized users.

E.-J. Koh · D. S. Williams · J. Park · . · B.-H. Kang
Department of Microbiology and Cell Science,
University of Florida,
Gainesville, FL 32611, USA

L. Zhou · Y.-P. Duan
U.S. Department of Agriculture, Agricultural Research Service,
U.S. Horticultural Research Laboratory,
2001 South Rock Road,
Fort Pierce, FL 34945, USA

B.-H. Kang (✉)
Interdisciplinary Center for Biotechnology Research,
University of Florida,
Gainesville, FL 32611, USA
e-mail: bkang@ufl.edu

Introduction

Huanglongbing (HLB), also known as citrus greening, is a serious disease of citrus, causing substantial losses in citrus fruit production worldwide (da Graca and Korsten 2004). HLB is associated with a phloem-limited, Gram-negative, α-proteobacterium *Candidatus Liberibacter* (Bove 2006). Three species of *Candidatus Liberibacter* have been detected in citrus trees affected by HLB, and the species most widespread in North America is *Candidatus Liberibacter asiaticus* (Las) (Gottwald 2009). Symptoms of HLB include blotchy chlorosis/mottling of leaves, yellow shoot, vein corking, stunted growth, suppression of new root growth, and, most importantly economically, production of unmarketable fruits that are small, green, and lopsided, with aborted seeds (Brlansky et al. 2010). Early detection of Las/HLB is difficult because Las

concentration is low and its distribution is uneven in HLB-affected trees and because Las has not been able to culture to date and HLB symptoms have occasionally been confused with those from nutrient deficiencies (Li et al. 2006). It has been shown that HLB-symptomatic leaves accumulate excessive amounts of starch (Kim et al. 2009; Achor et al. 2010).

Starch accumulation in plant cells has often been associated with impairment of symplastic transport through plasmodesmata (PD). A maize mutant, sucrose export-deficient (*sxd1*) exhibits excessive starch accumulation in leaf chloroplasts and inhibition of symplastic transport between the bundle sheath and vascular parenchyma cells in leaf minor veins (Russin et al. 1996; Botha et al. 2000). Overexpression of tobacco mosaic virus (TMV) movement proteins interfered with photoassimilate export from source leaves in tobacco, and the increased level of carbohydrates in the leaves was associated with PD occlusion (Almon et al. 1997; Rinne et al. 2005). Recently, it was reported that inhibition of the symplastic spread of TMV resulting from overexpression of a PD-localized glycoprotein accompanies starch accumulation and photoassimilate retention in tobacco leaves, suggesting that symplastic transport is required for export of photoassimilate (Zavaliev et al. 2010).

The cell wall surrounding PD is enriched with callose, and high levels of callose inhibit transport through PD (Maule 2008). Callose synthesis in PD is induced by diverse biotic and abiotic stresses such as viral infection (Rinne and Schoot 2003; Roberts and Oparka 2003), metal toxicity (Sivaguru et al. 2000), cellular plasmolysis (Drake et al. 1978), and wounding (Radford et al. 1998). It has also been shown that mutant plants in which phloem transport is inhibited accumulate excessive callose around PD in their phloem cell wall (Botha et al. 2000; Maeda et al. 2006). Callose is utilized in the regulation of PD transport during normal plant development for rapid cell elongation and for the establishment of symplastic domains (Rinne et al. 2001; Ruan et al. 2001; Lucas et al. 2009).

Las is a phloem-inhabiting bacterium and could disrupt these cells. The retention of starch and sucrose in Las-infected (Las^+) citrus leaves suggests an impairment in photoassimilate export (Kim et al. 2009). We investigated phloem cells of Las^+ leaves using microscopy techniques. In Las^+ leaves, excessive callose formation was observed at PD in the phloem, and this callose deposition preceded increased starch accumulation. We demonstrated that photoassimilate export from source leaves is delayed and that symplastic transport into sieve tubes is retarded in Las^+ leaves. These results indicate that Las infection induces callose deposition in the phloem and suggest that many symptoms of HLB may arise from inhibited phloem transport.

Materials and methods

General reagents

All reagents, unless specified, were purchased from Sigma Chemical (St. Louis, MO).

Plant materials

In this study, leaves from healthy and HLB-infected citrus, *Poncirus trifoliate*, plants were used for SEM, aniline blue staining, and carboxyfluorescein diacetate (CFDA) dye transport assays; healthy and HLB-infected grapefruit (*Citrus xparadisi*) plants were used for TEM and for CO_2 pulse-labeling assays. All plants were grown in a standard greenhouse at the USDA-ARS Horticultural Research Lab in Ft. Pierce, FL, or in a plant containment facility at the University of Florida in Gainesville, FL. HLB-infected plants had been previously inoculated with Las by grafting with scions collected from diseased trees in the field. They had been maintained in the greenhouse for about 2 years before use.

Aniline blue staining and epifluorescence microscopy

Callose was detected after aniline blue staining as described in Ruzin (1999). Small samples from leaves were punched out with 3-mm (diameter) biopsy punches (Miltex, York, PA) and the sample discs were cut in half. One half was quickly transferred to FAA (37% formaldehyde/glacial acetic acid/95% ethanol/deionized water at a volume ratio of 50:5:10:35) for staining with aniline blue. The other half was dissected to extract DNA from leaf veins for Las detection by real-time PCR (see below). Leaf samples that were determined to be negative for Las infection by real-time PCR were classified as uninfected regardless of whether the samples were taken from uninfected or HLB-symptomatic trees. After a 2-h incubation in FAA, followed by washing in deionized water, the fixed samples were stained with 0.01% aniline blue (in 0.1 M phosphate buffer, pH 9.0) for 10 min. The stained samples were rinsed with deionized water, trimmed to remove ground tissues, and embedded in 6% low-melt agarose (Promega, Madison, WI). The embedded samples were sliced into 0.3-mm-thick cross-sections or longitudinal sections with a Vibratome (Leica Microsystems, Bannockburn, IL) and examined with an Olympus BH2 epifluorescent microscope (Center Valley, PA) using a 355- to 375-nm excitation filter, a 400-nm dichromatic mirror, and a 435- to 490-nm emission filter (Chroma Technology, Bellows Falls, VT). Nine to 12 leaf samples from each type of plants (Las^-, Las^+ non-chlorotic, and Las^+ chlorotic) were examined; representative images are shown in Fig. 1.

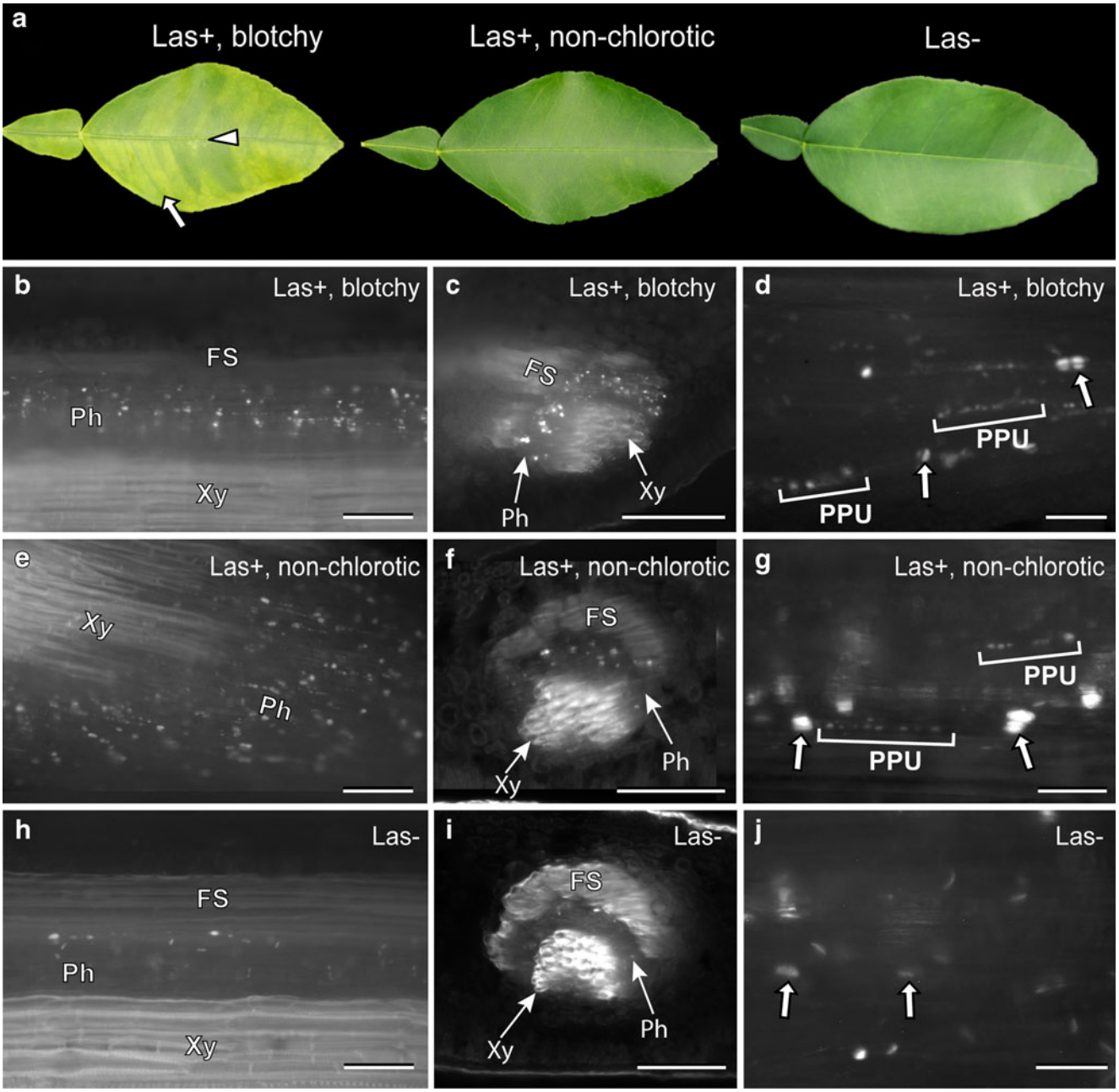

Fig. 1 Callose deposition in sieve tubes of Las^{+} leaf veins. **a** Blotchy chlorotic Las^{+}, non-chlorotic Las^{+}, and uninfected grapefruit leaves. Midvein and lateral vein are marked with an *arrowhead* and with an *arrow*, respectively. **b**–**j** Aniline blue staining of callose in lateral vein samples of Las^{+} blotchy chlorotic (**b**–**d**), Las^{+} non-chlorotic (**e**–**g**), and negative for Las infection (**h**–**j**) (Las^{-}) leaves. For each sample, longitudinal (**b**, **d**, **e**, **g**, **h**, **j**) and cross-section (**c**, **f**, **i**) images are shown. In higher magnification images (**d**, **g**, **j**), linear small fluorescent spots indicating plasmodesmata pore units (*PPUs*) are marked with *brackets*, and fluorescence from sieve plate callose is marked with *arrows*. *FS* fiber strand, *Ph* phloem, *Xy* xylem. *Scale bars*, 100 μm (**b**, **e**, **h**); 500 μm (**c**, **f**, **i**), 20 μm (**d**, **g**, **j**)

Transmission electron microscopy and immunogold labeling

It has been reported that callose deposition around PD occurs in plant specimens as a wound reaction when specimens are dissected and fixed for TEM imaging (Hughes and Gunning 1980; Radford et al. 1998). To suppress this wound response, 0.5 mL of 0.1 mM 2-deoxy-D-glucose (a callose synthase inhibitor) was applied to uninfected, Las^{+} non-chlorotic, and Las^{+} mottled leaves near vein by pressure injection. After 3 h, vascular and ground tissue samples were dissected from the leaves with either a biopsy punch or a single-edge razor blade. The dissected samples were quickly placed in a primary fixative

of 2.5% glutaraldehyde and 2.5% formaldehyde in 0.1 M cacodylate buffer (pH 7.2) and were fixed under vacuum at 4°C overnight. After rinsing in 0.1 M cacodylate buffer three times, the samples were secondarily fixed in 2% osmium tetroxide in 0.1 M cacodylate buffer at 4°C overnight. After rinsing four to five times in deionized water, the samples were treated with 1% aqueous uranyl acetate at room temperature. Dehydration was carried out in a graduated ethanol series to 100% ethanol and then 100% acetone. The dehydrated samples were then slowly and progressively infiltrated with Spurr's epoxy resin, mixed with acetone, to 100% Spurr's resin, and were polymerized at 60°C. The samples were briefly irradiated with microwave under vacuum at each step to aid penetration and infiltration using a Pelco Biowave 34700 microwave oven (Ted Pella, Redding, CA). Polymerized samples were sectioned on an MT-6000-XL ultramicrotome (RMC, Tucson, AZ). Sections were collected on formvar-coated slot or 100-mesh copper grids and post-stained with Reynold's lead citrate and 2% aqueous uranyl acetate. Five to eight leaf sample blocks from each type of plants (Las^-, Las^+ non-chlorotic, and Las^+ chlorotic) were examined by TEM.

For immunogold labeling, the dissected leaf samples were fixed in 4% formaldehyde and 0.5% glutaraldehyde in 0.1 M cacodylate buffer and slowly dehydrated through a graduated ethanol series to 100% ethanol followed by slow and progressive infiltration with L.R. White (medium grade) acrylic resin mixed with ethanol to 100% L.R. White resin. The samples were polymerized in a 50°C oven and sectioned on an Ultracut UCT ultramicrotome (Leica Microsystems). Sections were collected on formvar-coated gold or nickel slot grids, and callose was localized with a callose antibody (cat. no. 400-2, Biosupplies, Parkville, Australia; antibody dilution=1/200, *v*/*v*). Immunogold labeling was carried out as described in Kang and Staehelin (2008).

Sections were viewed on an H-7000 transmission electron microscope at 100 KV (Hitachi America, Inc., Schaumburg, IL) equipped with an SIS Veleta digital camera (Olympus). The average diameters of callose aggregates at PD were calculated from 40 plasmodesmata pore units (PPUs) from Las^+ and Las^- vein samples. Diameters of the PPUs were measured from transmission electron micrographs using the ImageJ 1.38X National Institute of Health, USA (http://rsb.info.nih.gov/ij/), program.

CFDA uptake assay

For the fluorescent dye diffusion experiment, approximately 300 μL of CFDA in 20 mM phosphate buffer (pH 7.2) was applied to citrus leaves by pressure injection of the abaxial leaf surface with the blunt end of a 1-mL Luer-Lok™ syringe (BD, Franklin Lakes, NJ). Ten green leaves from two uninfected plants, ten green leaves from two Las^+ plants, and ten chlorotic leaves from three Las^+ plants were injected, and the plants were maintained under identical greenhouse conditions, with 16/8 h of light/dark at 28°C. All injected leaves were collected 2 days after injection and were examined with a SZX12 fluorescence stereomicroscope equipped with a DP digital imaging system (Olympus). After imaging, the presence or absence of Las in each sample was tested by the PCR method described below. To quantify fluorescence, we opened micrographs in the ImageJ 1.38X National Institute of Health, USA (http://rsb.info.nih.gov/ij/), program. Ground and vascular tissues were segmented in approximately 1× 1-cm regions in each micrograph, and the average intensity values of the segmented areas (in the green channel) were obtained with the Measure function of the ImageJ program.

Scanning electron microscopy

Sample preparation for scanning electron microscopy (SEM) was carried out by essentially the same procedure as detailed in Mullendore et al. (2010). Leaf veins were excised with a scalpel and were placed directly into liquid nitrogen (LN_2). The frozen leaf vein samples were placed into cryovials containing freeze substitution media (100% ethanol) in LN_2. The cryovials were transferred to a −20°C freezer and incubated for 24 h. The freeze-substituted samples were warmed up to room temperature and washed three times with deionized water. The washed vein samples were chopped into approximately 1-mm^2 pieces and were partially digested in a Tris–HCl buffer (50 mM, pH 8.0) containing 0.1% protease K (Invitrogen, Carlsbad, CA), 8% Triton X-100, and 1.5 mM calcium acetate. The samples were incubated at 55°C on a Thermomixer (Eppendorf, Hauppauge, NY) for 3 days (with shaking at 350 rpm). The digestion solution was replaced and the samples were incubated for another 3 days. After inactivating the protease K with 100% ethanol, the samples were placed in an amylase solution (0.1% amylase in 10 mM Tris–HCl, pH 7.0) and were incubated at 60°C for 24 h.

The samples were subsequently dehydrated in a graduated ethanol series and were dried with a critical point drier (EM CPD030, Leica Microsystems). Dried samples were mounted on adhesive tabs on aluminum specimen mounts (Ted Pella) and Au/Pd sputter-coated (DeskII, Denton Vacuum, Moorestown, NJ). High-resolution digital micrographs were acquired with a field emission scanning electron microscope (S-4000, Hitachi America, Inc.). From the micrographs, sieve pore diameters were measured using the ImageJ (1.38X National Institute of Health,

USA; http://rsb.info.nih.gov/ij/) program. In oblique views, sieve pores are ellipses; their largest transverse diameters were measured. For the charts in Fig. 3e, 415 sieve pores (220 from uninfected and 195 from Las-infected leaf samples) were measured. Ten samples from Las^- plant leaves and ten samples from Las^+ chlorotic plant leaves were examined by SEM.

$^{14}CO_2$ pulse-labeling experiments

Two uninfected and two Las^+ grapefruit plants were transferred from a growth chamber into a laboratory hood and were grown for 3 days with fluorescent light illumination of 150 μE/m^2 s^1. Fully expanded source leaves on uninfected and Las-infected plants (six leaves from each plant) were enclosed in transparent polyethylene bags (Ziploc bags, S.C. Johnson, Racine, WI) which were sealed around the petiole using modeling clay (Crayola, Easton, PA). A single leaf was enclosed in each bag and a microcentrifuge tube was affixed with plastic tapes inside of each bag. Using a syringe, 5 μCi (0.2 mL) $NaH^{14}CO_3$ (Sigma) was injected into the microcentrifuge tube in the bag, followed by an equal volume of 0.1 N HCl. After tapping the microcentrifuge tube gently to mix the acid and $NaH^{14}CO_3$, the needle puncture holes were sealed with plastic tape. After 2 h of incubation, the polyethylene bags were removed and leaves were excised and dried in a 60°C oven for 6 h. Leaves were also collected and dried after 24- and 48-h chase periods. The dried leaves were exposed to a phosphorimaging screen (Kodak, Rochester, NY) for 6 h at room temperature and the screen scanned with a Personal Molecular Imager scanner (Bio-Rad, Hercules, CA) operated with the Quantity One program (ver. 4.6.9, Bio-Rad). The chart in Fig. 5a was prepared from the quantification of ^{14}C in the labeled leaves by liquid scintillation counting (LSC). The ^{14}C-labeled leaves were placed in scintillation counting vials after drying and were submerged in a scintillation cocktail (ScintiVerse, Fisher Scientific). ^{14}C radioactivity from each vial was measured with an LS6500 multipurpose liquid scintillation counter (Beckman, Brea, CA). At each time point, four leaves were sampled. One leaf was saved for autoradiography and the other three leaves were analyzed by LSC. Unit counts per minute (CPM) were calculated by dividing LSC CPM by the leaf surface area (square centimeters). ^{14}C release rate was calculated after setting the average unit count just after labeling (0 h) at 100%.

PCR detection of *Ca. Liberibacter asiaticus*

Total DNA samples were extracted from citrus leaf veins following the manual instructions for a DNeasy Plant Mini Kit (Qiagen, Valencia, CA), and their concentrations were measured with a NanoDrop spectrophotometer (Thermo Scientific, Wilmington, DE). Las bacterial DNA was detected by means of the TaqMan real-time PCR amplification protocol with a 7500 Real-Time PCR System (Applied Biosystems, Foster City, CA). Las-specific primers, HLBas, HLBr, and HLBp (Li et al. 2006), were used in a 25-μL reaction volume containing 12.5 μL of Taqman PCR master mix (Applied Biosystems), 250 nm of each primer, 150-nm probe, and about 100 ng of template DNA. The amplification protocol was 95°C for 10 min, followed by 40 cycles at 95°C for 15 s each, and one cycle at 60°C for 1 min.

Results

Callose formation at plasmodesmata pore units and sieve plates in the Las^+ leaf vein

Sieve elements and companion cells constitute the phloem and are symplastically connected by PPUs between companion cells and sieve elements and sieve pores between sieve elements. We compared callose levels by epifluorescence microscopy, after staining with aniline blue, in the phloem from Las-infected (Las^+; Fig. 1a) leaf samples to those in phloem from leaf samples where no Las was detected by PCR (Las^-; Fig. 1a).

Small fluorescent dots were seen in lines along the phloem cells in Las^+ chlorotic blotchy leaves (Fig. 1b–d); the dots correspond to callose from PPUs in sieve tubes (Fig. 2). The intense staining indicates that callose is enriched in PPUs and sieve plates of the Las^+ phloem tissue. To determine whether the callose deposition around PPUs in the Las^+ phloem cell wall occurs before leaf chlorosis, non-chlorotic Las^+ leaves were examined after aniline blue staining. The PPUs in the green Las^+ leaves were stained at levels similar to the PPUs in the chlorotic Las^+ leaves, indicating that the callose deposition occurs prior to chloroplast breakdown (Fig. 1e–g). Sieve plates in Las^- samples were stained with aniline blue, but callose staining in PPUs was rarely detected (Fig. 1h–j).

Excessive callose accumulation at PPUs in the Las^+ phloem

We performed TEM and immuno-TEM analyses to localize callose in the Las^+ phloem cells. Occasionally, copious electron-lucent aggregates were seen on the cell walls of sieve elements in Las^+ vein samples (Fig. 2a). They were determined to be callose deposits around PPUs because (1) desmotubules were identified at the centers of the material (Fig. 2b, f) and (2) the material was heavily labeled with an anti-callose antibody (Fig. 2c, d). The callose aggregates had an average diameter of 320 nm (SD = 62 nm) and

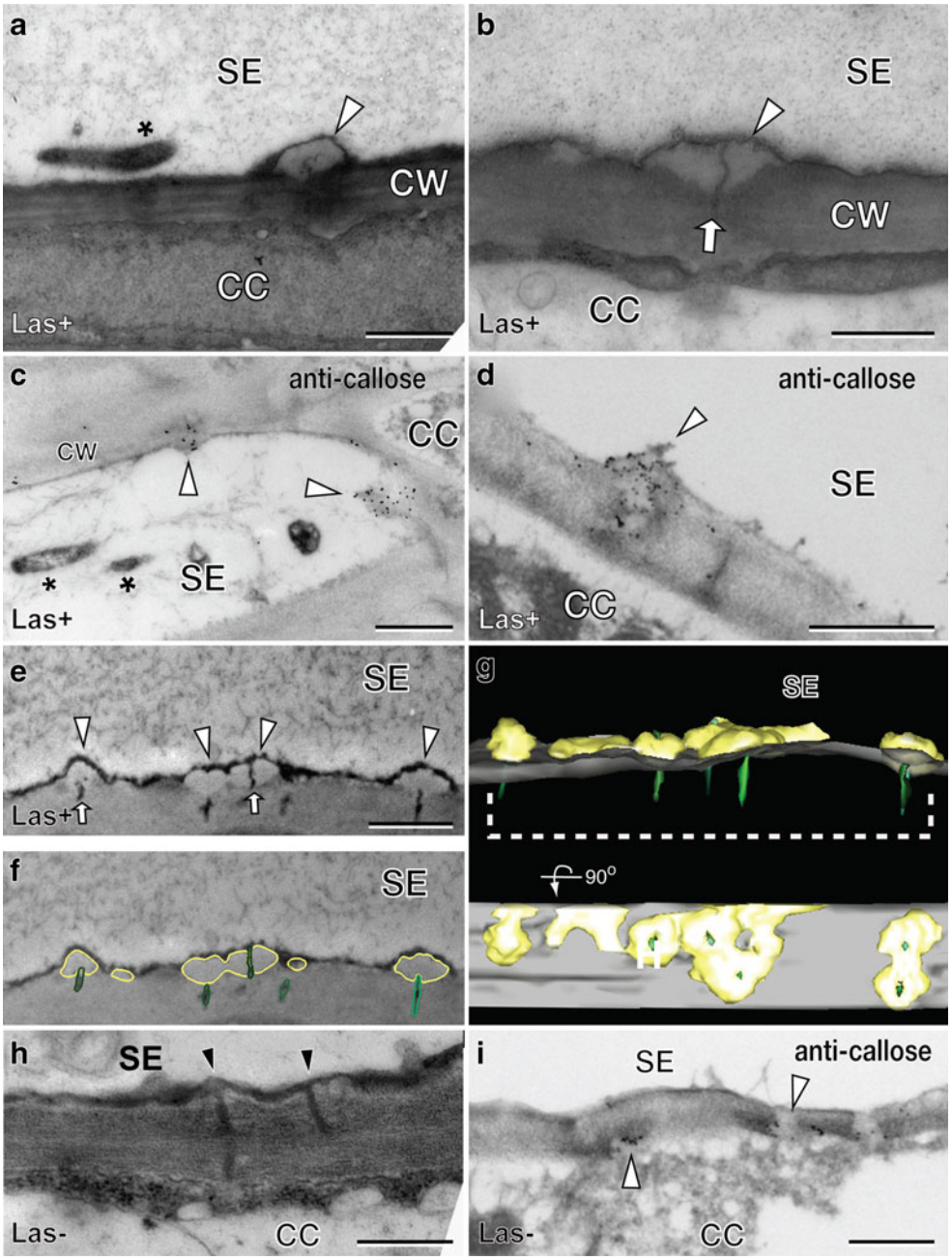

Fig. 2 Transmission electron micrographs and 3D reconstruction of Las$^+$ sieve elements (**a**, **b**) PPUs with excessive callose (*arrowheads*) in Las$^+$ leaf phloem cells. A Las cell is marked with an *asterisk* in **a**. Note a desmotubule (*arrow*) surrounded by a callose deposit in **b**. **c**, **d** Immunogold labeling of callose in phloem cells of Las$^+$ samples. PPUs with raised callose collars are marked with *arrowheads*. *Asterisks* in **c** indicate Las cells. **e**–**g** Three-dimensional reconstruction of PPUs and their callose. Desmotubules, callose, and the sieve element surface were outlined in 11 consecutive sections and rendered into 3D models. An electron micrograph from the serial sections and the outlines of desmotubules (*green*) and callose (*yellow*) in the micrograph are shown in **e** and **f**, respectively. **g** Side view and a top view of the 3D model. **h** Electron micrograph of phloem cells in an uninfected leaf. **i** Immunogold labeling of callose in phloem cells of an uninfected leaf. *SE* sieve element, *CC* companion cell, *CW* cell wall. *Scale bars*, 500 nm

bulged out into the sieve element. When a group of adjacent callose-accumulating PPUs was reconstructed into 3D models from serial section micrographs, the callose deposits were seen to merge and form large masses (Fig. 2g). When callose accumulation in Las$^+$ and Las$^-$ samples were compared in thin sections, PPUs with callose deposits thicker than 200 nm were approximately four times more abundant in the Las$^+$ phloem cells than in the Las$^-$ phloem cells (Table 1). PPUs in uninfected vein samples had thinner callose collars (<200 nm in diameters) and were associated with lower numbers of anti-callose immunogold particles (Fig. 2h, i). In addition to callose deposition in the PPU, collapsed phloem cells were observed in the Las$^+$ leaf veins (Electronic supplementary materials (ESM) Fig. S1).

Table 1 Correlation between Las infection and callose deposition around PPUs in the phloem

Las infection	Detection of aniline blue staining in the phloem	PPUs with excessive callose seen in TEM[a]
Positive	Detected	31 (89)
Negative	Not detected	4 (55)

[a] Numbers of PPUs surrounded by callose with diameters larger than 200 nm. Total numbers of PPUs examined in the TEM micrographs are indicated in parentheses

Callose formation in the sieve plates reduces sieve pore sizes, but does not occlude sieve pores

Aniline blue staining of Las$^+$ phloem tissues indicated that callose accumulates not only around PPUs but also in sieve plates (Fig. 1). We therefore examined callose formation in sieve pores with a SEM method recently developed by Mullendore et al. (2010).

Figure 3 shows the scanning electron micrographs of sieve plates in Las$^-$ and Las$^+$ leaves. The images are cross-

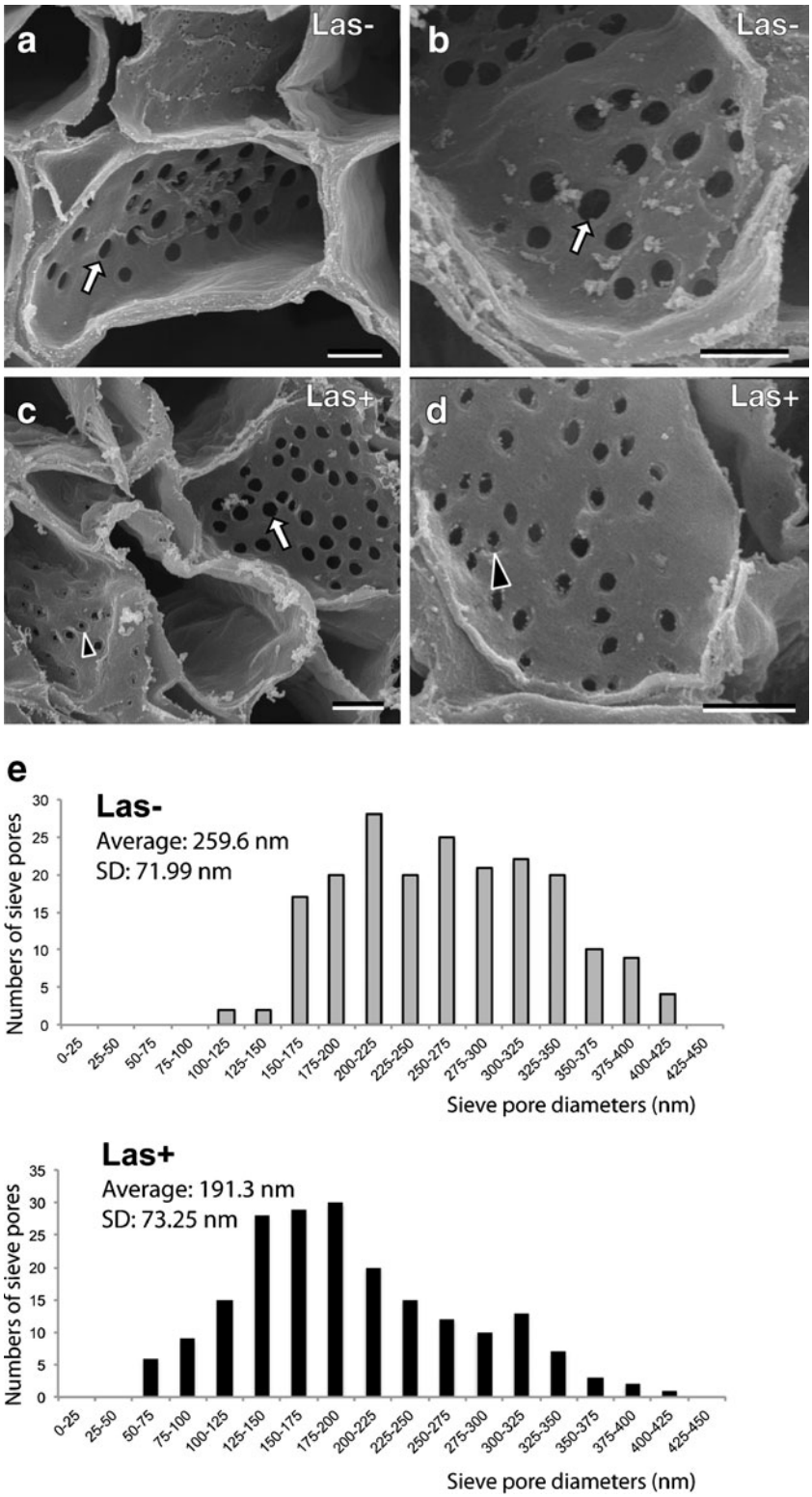

Fig. 3 Scanning electron micrographs of sieve plates in leaf veins negative (Las$^-$) and positive (Las$^+$) for Las infection. **a**–**d** Sieve plates in uninfected leaf veins (**a**, **b**) and Las$^+$ leaf veins (**c**, **d**). Regular sieve pores are marked with *arrows* in **a** and **b**. Not only normal-looking sieve pores (*arrows*) but also abnormally small sieve pores (*arrowheads*) are seen in Las$^+$ leaf veins (**c**, **d**). **e** Histograms of sieve pore diameters in Las$^-$ (*top panel*) and in Las$^+$ (*bottom panel*) leaf phloem. Diameters of 220 and 195 sieve pores were measured in Las$^+$ and in Las$^-$ specimens, respectively. The average sieve pore diameter in the Las$^+$ phloem is smaller than that in the Las$^-$ phloem. *SD* standard deviation. *Scale bars*, 1 μm

sections of leaf vascular tissues in which sieve pores are readily discerned. Sieve pores were seen as circular or elliptical pits, depending on the orientation of the sieve plates to the cut. Sieve pore diameters ranged from 120 to 418 nm in the Las$^-$ phloem samples (Fig. 3a, b); their average diameter was calculated to be 259.6 nm (Fig. 3e). Abnormally small pores (pores of which diameters are smaller than 100 nm) were observed in the Las$^+$ leaf veins (Fig. 3c, d). Their average sieve pore diameter measured 191.3 nm (52–415 nm; Fig. 3e), indicating that sieve pores have been constricted by callose accumulation in the sieve plate. However, we did not find sieve pores that were completely occluded by callose in Las$^+$ phloem samples.

Symplastic transport of a fluorescent dye into the vein is inhibited in Las$^+$ leaves

Callose formation around PPUs in Las$^+$ leaves may inhibit the symplastic flow of solutes from companion cells into sieve tubes, thereby reducing the phloem loading efficiency. To test this notion, we injected a symplast fluorescent tracer, CFDA, into non-vascular areas in mature leaves and monitored transport of the dye into vascular tissue after 48 h. In Las$^-$ samples, CFDA (Fig. 4a) had been imported into the veins, well visualizing leaf veins. In contrast, fluorescence in minor veins was often dimmer than in the surrounding non-vascular tissue in Las$^+$ leaf samples,

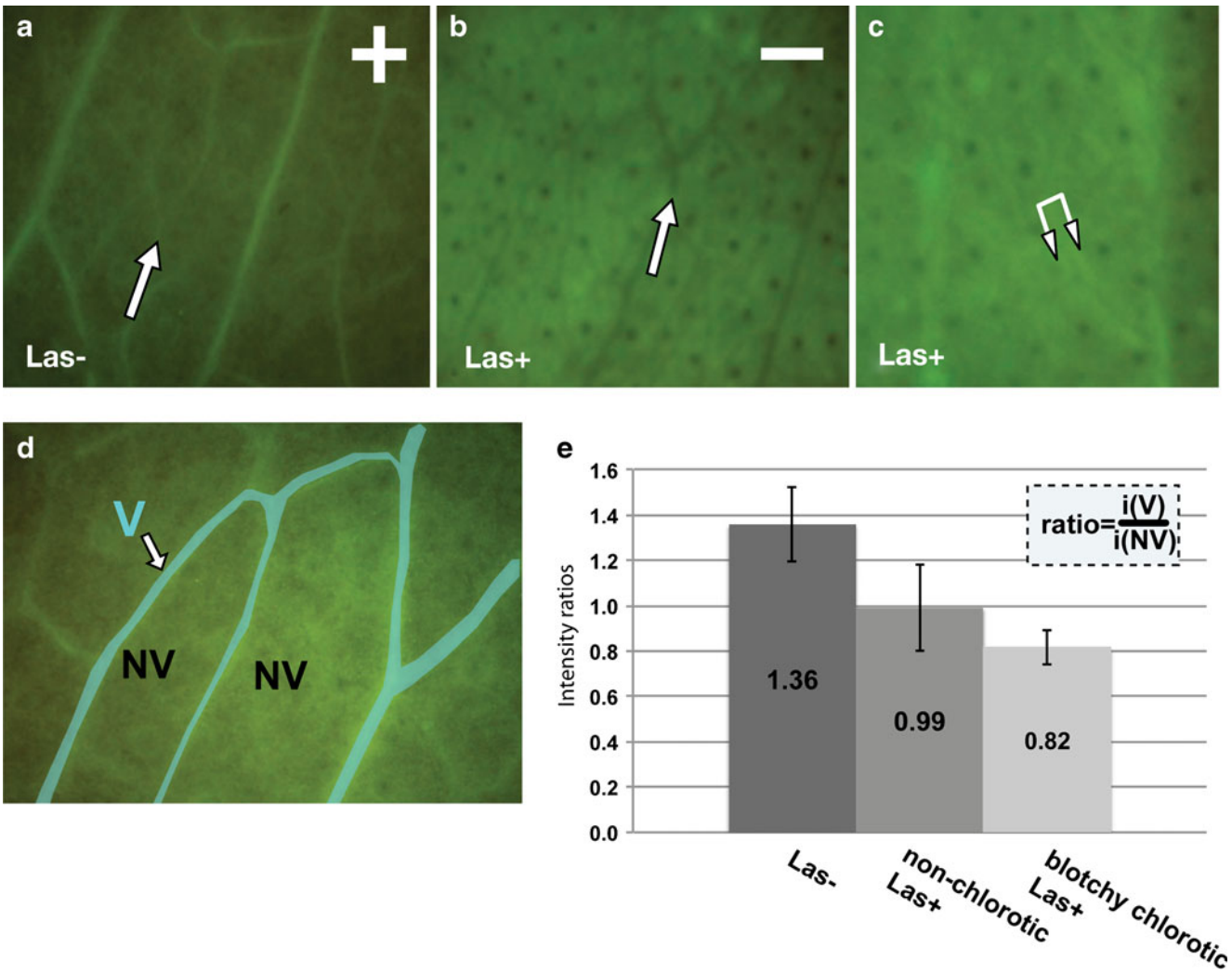

Fig. 4 Inhibited transport of a symplastic dye into the vascular tissue in Las-infected leaves (**a**, **b**). Examples of leaves in which CFDA is concentrated in the vein (**a**) and excluded from the vein (**b**). **c** CFDA was observed to accumulate immediately outside of the vein in Las$^+$ leaf samples (*double arrowheads*), suggesting an inhibition in phloem loading. **d** Vascular (*V*) and non-vascular (*NV*) tissues were outlined to calculate average fluorescence intensity values. **e** Graph showing average fluorescence intensity ratios between the vascular and non-vascular tissues (*inset*). Ratios from six leaves were averaged for each of the three sample types (Las$^-$, non-chlorotic Las$^+$, and blotchy chlorotic Las$^+$). More CFDA is translocated to veins in Las$^-$ leaves than in Las$^+$ leaves. *Numbers* and *error bars* in the each *column* denote average ratios and standard deviations, respectively

indicating that CFDA remained in the non-vascular tissue (Fig. 4b). In Las^+ leaves, CFDA accumulated in cells along the vein, but not in the vein (Fig. 4c). These results suggest that symplastic transport from the non-vascular tissue into the vascular tissue is impaired in Las^+ leaves. When ratios of vascular fluorescence intensity to non-vascular fluorescence intensity were calculated in Las^-, Las^+ non-chlorotic, and Las^+ chlorotic leaf samples, CFDA accumulation was approximately 1.2-fold higher in vascular tissue in the Las^- samples, whereas the ratio is reversed in chlorotic blotchy Las^+ samples (Fig. 4d, e).

Delayed export of ^{14}C radioactivity after $^{14}CO_2$ labeling in Las-infected citrus leaves

We carried out CO_2 pulse-labeling experiments to determine whether Las infection interferes with photoassimilate export from source leaves. Fully expanded source leaves of Las^+ trees and of uninfected trees were labeled with $^{14}CO_2$ for 2 h, and ^{14}C radioactivity levels in the leaves were monitored at 24 and 48 h after the labeling (Fig. 5a). Eighty-one percent (SD = 5.3%) of ^{14}C measured at time 0 disappeared from uninfected leaves within 24 h, while only 46% (SD = 22%) of radioactivity was released from Las^+ leaves. At 48 h after labeling, Las^+ leaves still retained 29% (SD = 13%) of ^{14}C measured at time 0. The delayed export of fixed ^{14}C from the Las^+ leaves suggests that the starch buildup in the chloroplasts of Las^+ leaves may have resulted from the delayed translocation of photosynthates. Stronger labeling by $^{14}CO_2$ and impaired export of ^{14}C were also indicated in the autoradiographic images of ^{14}C-labeled Las^+ leaves (Fig. 5b).

Discussion

Our results provide evidence that callose formation in sieve tubes in citrus plants infected with Las could lead to a restriction of phloem transport. Las is a fastidious phloem-limited bacterium, and excessive callose deposition in the phloem is likely a plant defense reaction to the bacterium, as seen in other instances of pathogen infection in plant cells (Roberts and Oparka 2003). Titers of the Las bacterium in citrus trees are so low that it has been problematic to detect Las consistently (Li et al. 2006). The low titers of Las combined with evidence of symplastic transport inhibition in HLB-infected trees suggest that HLB symptoms are related to the phloem transport inhibition induced by the infection rather than by direct destruction of the phloem by Las cells.

Inhibition of phloem transport and HLB symptoms

Surplus energy-rich carbon compounds produced in source tissues are transported to sink tissues by way of the phloem, primarily as sucrose. This distribution of carbon and energy across the plant body is called carbon partitioning, and the process is critical for normal plant development (Braun and Slewinski 2009). Heterotrophic sink organs such as fruits, seeds, and roots and rapidly growing meristematic tissues are sustained by sucrose supplied from photosynthetic source tissues. The inhibition of photoassimilate export and the subsequent starch accumulation in the Las^+ leaves suggest that Las infection perturbs normal carbon partitioning. Mutant or transgenic plants exhibiting defective carbohydrate export from their leaves often present with excessive starch accumulation, stunted growth, poor root development, and

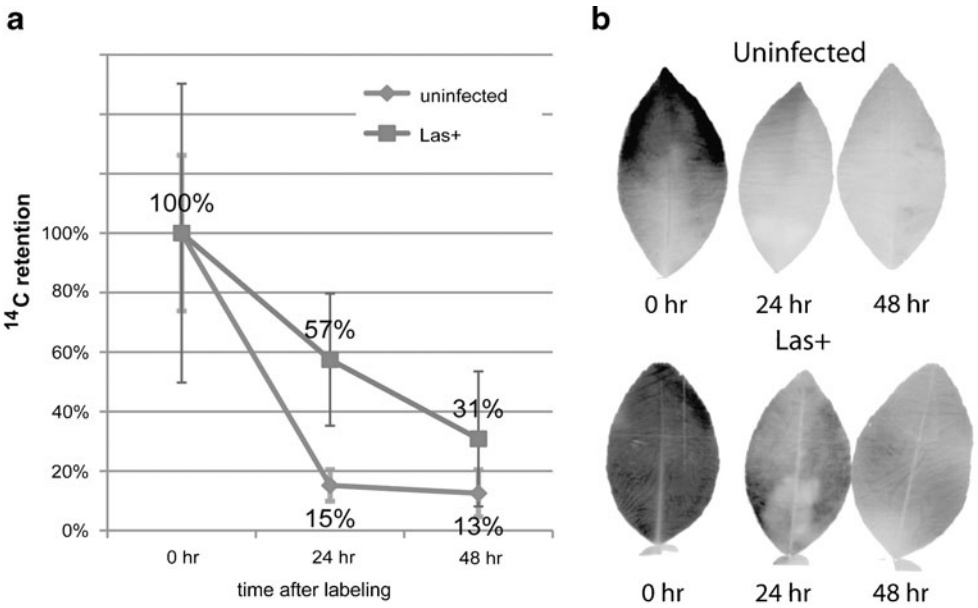

Fig. 5 $^{14}CO_2$ pulse labeling in Las-infected leaves. **a** Release of ^{14}C radioactivity from uninfected (*circle*) and non-chlorotic Las^+ (*square*) leaves. Relative amounts of ^{14}C retained after 24 and 48 h were plotted after setting ^{14}C radioactivity at 0 h to 100%. For each leaf, the counts per minute (cpm) value was divided by the surface area (counts per minute per square centimeter) because leaf sizes were not identical (ESM Table S1). The *error bars* at each time point indicate standard deviation (SD) values. **b** Autoradiograph of grapefruit leaves 0, 24, and 48 h after $^{14}CO_2$ labeling. Levels of radioactivity are stronger in Las^+ leaves than in Las^- leaves at each time point

aberrant seed/fruit development (Russin et al. 1996; Rinne et al. 2005; Kronberg et al. 2007; Ma et al. 2008; Zavaliev et al. 2010). These phenotypes are analogous to the symptoms of HLB infection (Brlansky et al. 2010).

Chlorotic Las$^+$ leaves suffer vein corking caused by the collapse of sieve tube cells (ESM Fig. S1). Unlike xylem vessels, sieve elements are not dead cell wall tubes. Their survival is dependent on companion cells with which sieve elements exchange macromolecules (van Bel et al. 2002). Callose constriction of the PPUs between sieve elements and companion cells inhibits symplastic trafficking that sieve elements rely on. Prolonged block of the macromolecular transport results in the death of sieve elements, contributing to the severity of Las pathogenicity.

Constriction of sieve pores in the Las$^+$ leaf phloem

Kim et al. (2009) and Achor et al. (2010) demonstrated by TEM that sieve pores in the midvein tissues of Las$^+$ leaves accumulate callose. Rapid plugging of sieve pores is a plant defense response to plant-feeding pests and to mechanical wounding in order to minimize the loss of concentrated photoassimilates from the phloem. The plugging is the result of rapid callose deposition around and of P protein being drawn into sieve pores. Unfortunately, this rapid wound reaction impedes the ultrastructural characterization of sieve elements by TEM because tissue dissection and chemical fixation trigger a similar artifactual obstruction of sieve plates (Evert 1982). This raises the question of whether previously reported sieve pore obstruction is a consequence of Las infection or of microscopy processing artifact, or both.

To address the rapid callose formation problem, we fixed our samples by freezing, to stop all enzymatic activity, including that of callose synthases, almost instantly. In addition, by utilizing SEM after clearing sieve tubes of their cytoplasm, we were able to visualize entire sieve plates in 3D, facilitating the measurement of hundreds of sieve pore diameters. Sieve pore diameter is an important structural determinant of conductivity through the sieve tube. The average reduction in pore size in Las$^+$ leaves suggests that long-distance translocation of photoassimilate is impeded (Thompson and Holbrook 2003).

Callose deposition at the PD induced by Las infection

It has been shown that either developmental signals or biotic/abiotic stresses can trigger callose synthesis around PD and that increased deposition of callose constricts the desmotubule. A line of evidence suggests that cellular redox status is involved in the regulation of callose synthesis around PD. Mutant plants in which the biosynthesis of vitamin E, a compound that protects against oxidative stress, is inhibited display increased levels of callose associated with PD in the vein cell wall and slowed photoassimilate export (Botha et al. 2000; Hofius et al. 2004; Maeda et al. 2006). Recently, an *Arabidopsis* mutant, *gfp arrested trafficking* 1 (*gat1*), in which unloading of GFP from the phloem is defective, was identified. *Gat1* encodes a protein involved in regulation of the cellular redox state and the *gat1* mutant accumulated not only reactive oxygen species (ROS) but also callose in the phloem (Benitez-Alfonso et al. 2009).

ROS generation is a plant defense mechanism (Torres et al. 2006). Plant cells invaded by a pathogen produce ROS rapidly, which results in diverse consequences, including membrane lipid oxidation, generation of toxic compounds, and hypersensitive reaction. Accepting that PD permeability is influenced by an increase in ROS (Benitez-Alfonso and Jackson 2009), it is possible that Las infection could trigger ROS production which, in turn, promotes callose synthesis at PD.

Acknowledgments We are grateful to Dr. Karen Koch (University of Florida) and her lab assistants for their help in $^{14}CO_2$ pulse labeling. We also thank Dr. Rob Ferl (University of Florida) and Dr. Tony Romeo (University of Florida) for allowing us to use their fluorescence stereomicroscope and phosphorimager scanner, respectively. We are indebted to Dr. Dean Gabriel (University of Florida) for the use of his citrus plants in the University of Florida Plant Containment Facility. We thank Dr. Mullendore (Washington State University) for his advice in carrying out scanning electron microscopy of sieve pores. This work was supported by the Florida Citrus Production Research Advisory Council (grant no. 113 to B-H. K.) and by the United States Department of Agriculture, (NIFA Award no. 2010-34446-21694 to B-H. K.)

Conflict of Interest The authors declare that they have no conflict of interest.

References

Achor D, Etxeberria E, Wang N, Folimonova SY, Chung K, Albrigo L (2010) Sequence of anatomical symptom observations in citrus affected with huanglongbing disease. Plant Pathol J 9:56–64

Almon E, Horowitz M, Wang HL, Lucas WJ, Zamski E, Wolf S (1997) Phloem-specific expression of the tobacco mosaic virus movement protein alters carbon metabolism and partitioning in transgenic potato plants. Plant Physiol 115:1599–1607

Benitez-Alfonso Y, Jackson D (2009) Redox homeostasis regulates plasmodesmal communication in *Arabidopsis* meristems. Plant Signal Behav 4:655–659

Benitez-Alfonso Y, Cilia M, San Roman A, Thomas C, Maule A, Hearn S, Jackson D (2009) Control of *Arabidopsis* meristem development by thioredoxin-dependent regulation of intercellular transport. Proc Natl Acad Sci U S A 106:3615–3620

Botha CEJ, Cross RHM, van Bel AJE, Peter CI (2000) Phloem loading in the sucrose-export-defective (SXD-1) mutant maize is limited by callose deposition at plasmodesmata in bundle sheath–vascular parenchyma interface. Protoplasma 214:65–72

Bove JM (2006) Huanglongbing: a destructive, newly-emerging, century-old disease of citrus. J Plant Pathol 88:7–37

Braun DM, Slewinski TL (2009) Genetic control of carbon partitioning in grasses: roles of sucrose transporters and tie-dyed loci in phloem loading. Plant Physiol 149:71–81

Brlansky RH, Dewdney ME, Rogers ME (2010) Florida citrus pest management guide: huanglongbing (citrus greening). Extension Digital Information Source (EDIS): PP-225 Department of Food and Resource Economics, University of Florida, Gainesville, FL

da Graca JV, Korsten L (2004) Citrus huanglongbing: review, present status and future strategies. Dis Fruits Veg 1:229–245

Drake GA, Carr DJ, Anderson WP (1978) Plasmolysis, plasmodesmata, and electrical coupling of oat coleoptile cells. J Exp Bot 29:1205–1214

Evert RF (1982) Sieve-tube structure in relation to function. Bioscience 32:789–795

Gottwald TR (2009) Current epidemiological understanding of citrus huanglongbing. Annu Rev Phytopathol 48:119–139

Hofius D, Hajirezaei MR, Geiger M, Tschiersch H, Melzer M, Sonnewald U (2004) RNAi-mediated tocopherol deficiency impairs photoassimilate export in transgenic potato plants. Plant Physiol 135:1256–1268

Hughes JE, Gunning BES (1980) Glutaraldehyde-induced deposition of callose. Can J Bot-Rev Canadienne De Botanique 58:250–258

Kang BH, Staehelin LA (2008) ER-to-Golgi transport by COPII vesicles in Arabidopsis involves a ribosome-excluding scaffold that is transferred with the vesicles to the Golgi matrix. Protoplasma 234:51–64

Kim JS, Sagaram US, Burns JK, Li JL, Wang N (2009) Response of sweet orange (*Citrus sinensis*) to '*Candidatus Liberibacter asiaticus*' infection: microscopy and microarray analyses. Phytopathology 99:50–57

Kronberg K, Vogel F, Rutten T, Hajirezaei MR, Sonnewald U, Hofius D (2007) The silver lining of a viral agent: increasing seed yield and harvest index in *Arabidopsis* by ectopic expression of the potato leaf roll virus movement protein. Plant Physiol 145:905–918

Li WB, Hartung JS, Levy L (2006) Quantitative real-time PCR for detection and identification of *Candidatus Liberibacter* species associated with citrus huanglongbing. J Microbiol Method 66:104–115

Lucas W, Ham B, Kim J (2009) Plasmodesmata—bridging the gap between neighboring plant cells. Trends Cell Biol 19:495–503

Ma Y, Baker RF, Magallanes-Lundback M, Dellapenna D, Braun DM (2008) Tie-dyed1 and sucrose export defective1 act independently to promote carbohydrate export from maize leaves. Planta 227:527–538

Maeda H, Song W, Sage T, Dellapenna D (2006) Tocopherols play a crucial role in low-temperature adaptation and phloem loading in *Arabidopsis*. Plant Cell 18:2710–2732

Maule A (2008) Plasmodesmata: structure, function and biogenesis. Curr Opin Plant Biol 11:680–686

Mullendore D, Windt C, Van As H (2010) Sieve tube geometry in relation to phloem flow. Plant Cell 22:579–593

Radford J, Vesk M, Overall R (1998) Callose deposition at plasmodesmata. Protoplasma 201:30–37

Rinne P, Schoot C (2003) Plasmodesmata at the crossroads between development, dormancy, and defense. Can J Bot-Rev Canadienne De Botanique 81:1182–1197

Rinne P, Kaikuranta P, Van Der Schoot C (2001) The shoot apical meristem restores its symplasmic organization during chilling-induced release from dormancy. Plant J 26:249–264

Rinne PL, van den Boogaard R, Mensink MG, Kopperud C, Kormelink R, Goldbach R, van der Schoot C (2005) Tobacco plants respond to the constitutive expression of the tospovirus movement protein NS(M) with a heat-reversible sealing of plasmodesmata that impairs development. Plant J 43:688–707

Roberts AG, Oparka KJ (2003) Plasmodesmata and the control of symplastic transport. Plant Cell Env 26:103–124

Ruan YL, Llewellyn DJ, Furbank RT (2001) The control of single-celled cotton fiber elongation by developmentally reversible gating of plasmodesmata and coordinated expression of sucrose and K^+ transporters and expansin. Plant Cell 13:47–60

Russin WA, Evert RF, Vanderveer PJ, Sharkey TD, Briggs SP (1996) Modification of a specific class of plasmodesmata and loss of sucrose export ability in the sucrose export defective1 maize mutant. Plant Cell 8:645–658

Ruzin SE (1999) Staining. In: Ruzin SE Plant microtechnique and microscopy. Oxford University Press, New York, pp 87–116

Sivaguru M, Fujiwara T, Šamaj J, Baluška F, Yang Z, Osawa H, Maeda T, Mori T, Volkmann D, Matsumoto H (2000) Aluminum-induced 1→3-β-D-glucan inhibits cell-to-cell trafficking of molecules through plasmodesmata. A new mechanism of aluminum toxicity in plants. Plant Physiol 124:991–1005

Thompson MV, Holbrook NM (2003) Application of a single-solute non-steadystate phloem model to the study of long-distance assimilate transport. J Theor Biol 220:419–455

Torres M, Jones J, Dangl J (2006) Reactive oxygen species signaling in response to pathogens. Plant Physiol 141:373–378

van Bel AJE, Ehlers K, Knoblauch M (2002) Sieve elements caught in the act. Trends Plant Sci 7:126–132

Zavaliev R, Sagi G, Gera A, Epel BL (2010) The constitutive expression of *Arabidopsis* plasmodesmal-associated class 1 reversibly glycosylated polypeptide impairs plant development and virus spread. J Exp Bot 61:131–142